Analytica Chimica Acta 1124 (2020) 166–175

Contents lists available at ScienceDirect

Analytica Chimica Acta

journal homepage: www.elsevier.com/locate/aca

Highly sensitive detection of Pb^{2+} and Cu^{2+} based on ZIF-67/MWCNT/Nafion-modified glassy carbon electrode

Yueying Zhang [a], Hao Yu [a], Tong Liu [a], Weijia Li [a], Xidong Hao [a], Qi Lu [a], Xishuang Liang [a, *], Fengmin Liu [a], Fangmeng Liu [a], Chenguang Wang [a], Chunhua Yang [b], Hongqiu Zhu [b], Geyu Lu [a, **]

[a] State Key Laboratory on Integrated Optoelectronics, Key Laboratory of Gas Sensors, Jilin Province, College of Electronic Science and Engineering, Jilin University, 2699 Qianjin Street, Changchun, 130012, China
[b] School of Information Science and Engineering, Central South University, Changsha, 410083, China

HIGHLIGHTS

- A novel multiphase modification layer based on ZIF-67/MWCNT/Nafion was constructed.
- This modification layer greatly improved Pb^{2+} and Cu^{2+} sensing performance.
- The sensor displayed a low detection limit of 1.38 nM for Pb^{2+} and 1.26 nM for Cu^{2+}.

GRAPHICAL ABSTRACT

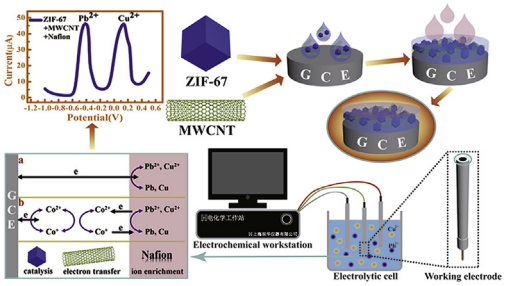

ARTICLE INFO

Article history:
Received 14 February 2020
Received in revised form
24 April 2020
Accepted 8 May 2020
Available online 14 May 2020

Keywords:
Multiphase modification layer
Electrochemical sensor
Heavy metal ion detection
GCE
Voltammetry

ABSTRACT

A series of different facile modification layers (MLs) was designed to gradually increase the electrochemical sensing performance of glassy carbon electrode (GCE) for simultaneously detecting Pb^{2+} and Cu^{2+}. ML designs were mainly a different combination of ZIF-67, MWCNT and Nafion, and their different electrochemical sensing performances were investigated by cyclic voltammetry (CV), electrochemical impedance spectroscopy (EIS), square wave stripping voltammetry (SWSV) and chronocoulometry. The fabricated sensor, which modified with ZIF-67/MWCNT and Nafion layer, exhibited the biggest response peak current to Pb^{2+} and Cu^{2+}. In addition, it displayed a wide linear detection range of 1.38 nM–5 μM for Pb^{2+} and 1.26 nM–5 μM for Cu^{2+}, a detection accuracy of about 1 nM for both Pb^{2+} and Cu^{2+}, and an excellent stability for both Pb^{2+} and Cu^{2+}. We also analyzed the real water sample taken from Changchun's Sanjia Lake and Yan Lake. We believe this ML design provides instruction for building high-performance electrochemical sensing systems.

1. Introduction

Heavy metal ions (HMIs), due to their high toxicity and non-biodegradability, have a major threat to human health [1–3]. For example, lead (Pb) intake affects adversely the central nervous system and the developing brain. And these effects have been found

* Corresponding author.
** Corresponding author.
E-mail addresses: liangxs@jlu.edu.cn (X. Liang), lugy@jlu.edu.cn (G. Lu).

https://doi.org/10.1016/j.aca.2020.05.023
0003-2670/

more terrible for children even under a safe concentration [4,5]. Although copper (Cu) is an essential element of the body, when being excessive, it will induce damage to the liver, gastrointestinal, and kidney [6]. Non-biodegradability means HMIs get the biggest enrichment in human beings with the progressive food chain. Therefore, monitoring HMIs in a low cost, facile and sensitive way is essential for human health. HMIs detection techniques are mainly atomic absorption spectrometry (AAS) [7], surface−enhanced Raman spectrometry (SERs) [8], UV−vis spectrophotometry [9], inductively coupled plasma mass spectrometry (ICP-MS) [10] and electrochemical sensors [11]. Compared to the others, electrochemical sensors have many unique features such as low cost, simple operation, portability, remarkable sensitivity, and low detection limit, which are significant for the on-site and routine monitoring HMIs. For electrochemical sensors, GCE has the characteristics of high chemical stability, wide potential applications, and easy modification. And it has been widely used as the working electrode in electrochemical sensors. Because the electrochemical reaction of heavy metal ions occurs at the interface between the working electrode and the electrolyte. The electrode modified material of GCE has a significant influence on the sensing performance.

Porous metal organic framework (MOF) consists of alternate organic moieties and metal ions/clusters. Metal nodes of the unsaturated coordination sites and abundant coordinative defect sites on the exterior solid surfaces make MOF have a good catalytic activity [12]. MOF is used as a good catalyst in many fields such as oxidative desulfurization [13], degradation of organic pollutants from wastewater [14], Dye Degradation [15], fast Knoevenagel condensation [16], etc. ZIF-67, made up of bridging 2-methylimidazolate anions and Co^{2+} cations, is one important subpart of MOF. At the same time, ZIF-67 with an easy-to-synthesize property has been found a good adsorption to HMIs [17−20]. Hence, we chose ZIF-67 as a modification material to build the electrochemical sensor for detecting HMIs. However, the poor conductivity and stability in water constrain its application in electrochemical sensors.

To overcome these defects, we introduced the multiwalled carbon nanotubes (MWCNTs) and Nafion membrane. MWCNT with an excellent conductivity has been used in many electrochemical sensors to promote electrons transfer and then improve the sensing performance [21−24]. Besides, Nafion, as a selectively permeable membrane, has a good adsorption for HMIs and good stability in solution. When the solvent of the Nafion solution is evaporated, a stable film is formed on the surface of the electrode to block the direct contact of ZIF-67 with air and solution, thereby improving the mechanical stability of the modified electrode. Nafion also has a good cation-exchange property and strong adsorption capacity [25,26]. Moreover, the use of multiple characteristics of the composite system to improve performance has been proven to be effective in various electrochemical systems, such as drug detection [27], gas detection [28], OER reaction [29] and full cell [30]. Therefore, MWCNT was used to improve the poor conductivity of ZIF-67 and Nafion was used to further stabilize the modification layer of ZIF-67/MWCNT. The synergy of the three materials ZIF-67/MWCNT and Nafion improves the sensing performance of GCE on Pb^{2+} and Cu^{2+}. Related work has not been reported in the previous literature.

In this work, Pb^{2+} and Cu^{2+} sensors based on ZIF-67/MWCNT and Nafion were fabricated. The research focused on the improvement of the electrochemical performance of ZIF-67 by MWCNT and Nafion. At the same time, the effects of different modification ways of Nafion on the sensing performance were studied. In addition, we have also studied the repeatability, anti-interference ability, reproducibility, stability, specificity, and recovery of the sensor.

2. Experiment section

2.1. Reagents

MWCNT was purchased from Xianfeng Nano Technology Co., Ltd., with a carboxyl content of 1.73 wt%. Other chemicals and reagents are all of analytical grade. For the choice of water samples, we chose commercial pure water and laboratory-prepared pure water (resistivity 18.2 MΩ cm), and conducted Inductively coupled plasma mass spectrometry tests (ICP-MS) on their Pb^{2+} and Cu^{2+} content to select a purer water sample to construct the detection system. Relevant ICP-MS test results were shown in Table S1(in the supporting information). At the same time, ICP-MS was used to test Pb^{2+} and Cu^{2+} content in real water samples.

2.2. Preparation of ZIF-67

ZIF-67 was synthesized according to previous studies [31]. Firstly, 1.164 g of $Co(NO_3)_2 \cdot 6H_2O$ and 1.314 g of 2-methylimidazole were separately dissolved in 100 mL of Methanol. Then poured $Co(NO_3)_2$ solution into 2-methylimidazole solution and stirred vigorously for 15 min. The mixed solution was left still at room temperature for 24 h. Finally, the obtained product was filtered with a 0.22 μm membrane and dried at 30 °C for 24 h.

2.3. Functionalization of MWCNT

In order to improve the dispersibility of MWCNT in water, MWCNT was pretreated with a mixture of nitric acid and sulfuric acid (volume ratio of 1:3). Specific steps were as follows: Firstly, 0.4 g MWCNT was added into 20 mL mixed acid solution. The suspension was then refluxed for 6 h with continuous stirring at 40 °C. It was then rinsed with water to reduce acidity and centrifugated until the pH was natural. Finally, the obtained product was dried at 30 °C in an oven.

2.4. Fabrication of ZIF-67, ZIF-67/MWCNT, ZIF-67/MWCNT/nafion modified electrodes

Firstly, ZIF-67 1.25 mg and MWCNT 1 mg were separately dispersed in 1 mL deionized water to obtain a uniformly dispersed suspension. 5 μL MWCNT suspension was then added into 95 μL ZIF-67 suspension and ultrasonicated for 5 min, obtaining the ZIF-67/MWCNT modified solution. Next, 2 μL Nafion was added into 8 μL ZIF-67/MWCNT modified solution and ultrasonicated for 5 min, obtaining the mixed modification of Nafion modified solution named mixed Nafion solution.

Prior to the modification, GCE was sequentially polished with Al_2O_3 powder having a particle size of 1 μm, 0.3 μm, and 0.05 μm. After rinsing with deionized water, CV characterization of the electrode was carried out in 5 mM $K_3Fe(CN)_6$ containing 1 M KCl at a potential range of −0.3 to 0.7 V to check the surface state of GCE. GCE was then ultrasonicated with dilute sulfuric acid, ethanol, and deionized water. Finally, GCE was dried with nitrogen and the corresponding modified materials were added. ZIF-67 and ZIF-67/MWCNT-modified electrodes were obtained by adding 8 μL ZIF-67 and ZIF-67/MWCNT suspension onto the electrode. Herein, to better understand the effect of Nafion, we design two kinds of Nafion modification ways: One is a mixed modified layer of ZIF-67/MWCNT and Nafion, and the other is a layered modified layer of ZIF-67/MWCNT and Nafion. The mixed modification of the Nafion modified electrode was obtained by adding 10 μL mixed Nafion solution. The layered modification of the Nafion modified electrode was obtained by adding 8 μL ZIF-67/MWCNT suspension and then adding 2 μL Nafion to the dried electrode surface. All the modified

electrodes were dried under an infrared baking lamp.

2.5. Electrochemical measurements

The three-electrode system was used for all electrochemical tests, where modified GCE (diameter: 3 mm) as the working electrode, Ag/AgCl (3 M KCl) as a reference electrode, and a platinum sheet as a counter electrode. 5 mM $[Fe(CN)_6]^{-3/-4}$ with 0.1 M KCl solution was used for CV and EIS measurements. 0.1 M different pH HAc-NaAc buffer solutions were used for SWSV measurements and prepared by mixing different ratios of 0.1 M HAc, 0.1 M NaAc, 0.1 M HCl and 0.1 M NaOH. The chronocoulometry test was performed in 0.1 M HAc-NaAc (pH 4.0) buffer solution containing 0.6 μM Pb^{2+} and Cu^{2+} at a deposition potential of −0.9 V.

2.6. Apparatus

The crystal structures of ZIF-67 and MWCNT were characterized by powder X-ray diffraction (XRD, D/max rA, Cu Kα radiation at wave length = 0.1541 nm). And field emission scanning electron microscopy (SEM, FEI Inspect F50) was used to record the surface morphology of modified materials. X-ray photoelectron spectroscopy (XPS) measurement was conducted in an American Thermo Fisher 250XI photoelectron spectrometer to determine the composition of ZIF-67. ICP-MS (PerkinElmer, NexLON 350D) was used to calibrate the HMIs content of solution samples.

3. Results and discussion

3.1. Crystal structure and morphological characterizations

XRD patterns of MWCNT and ZIF-67 were shown in Fig. 1(a) and (b). After the acid treatment, the XRD pattern of MWCNT is corresponding to the graphite carbon. The characteristic diffraction peak of graphite at $2\theta = 26.4^\circ$ is obvious, indicating the acid treatment didn't destroy the crystal structure of MWCNT. At the same time, the SEM images of MWCNT before and after acidification were shown in Figs. S1(a) and (b), respectively. The surface of MWCNT before acidification is smooth, but obviously roughens after acidification, which proves the successful functionalization of MWCNT according to the reported article [32]. Fig. S2 shows the FT-IR spectrometer of MWCNT after acidification. The stretching vibration of C=O and O-H can be found at 1647 cm^{-1} and 3220 cm^{-1} [23], demonstrating the existence of carboxyl and hydroxyl groups. As also shown in Fig. 1(b), all the characteristic peaks of the synthesized ZIF-67 are in good consistence with the simulated ZIF-67, demonstrating the successful synthesis of ZIF-67. The surface compositions and Co ions' valent states of ZIF-67 were further studied by XPS. Fig. 1(c), the full survey spectrum, confirms the existence of Co, N, C, and O of ZIF-67. As shown in the high-resolution spectrum of Co 2p (Fig. 1(d)), Two main peaks at 796.6 and 781.1 eV correspond to Co 2p1/2 and Co 2p3/2 respectively, which verifies the presence of Co(II) of ZIF-67. The other two peaks at 802.3 and 786.3 eV are typical Co^{2+} shakeup satellite peaks [33,34]. Therefore, cobalt in ZIF -67 exists in divalent form, consistent with previous reports [33,35].

SEM images characterize the morphology of the electrode modification suspension after ultrasonic treatment. As shown in Fig. 2(a) and (b), only a part of ZIF-67 still retains the polyhedral skeleton, while the other part is ultrasonically broken into small nanoparticles. MWCNT maintains its original tubular structure with a diameter of about 38.5 nm and is well dispersedly distributed without entanglement. After further mixing with ultrasonication, the morphology of ZIF-67/MWCNT was illustrated in Fig. 2(e) and (f). ZIF-67 is completely broken into nanoparticles and mixed with tubular MWCNTs. Due to the effect of ZIF-67 nanoparticles, there are many visible nanoparticles on the MWCNTs' surface and the diameter of MWCNTs increases to 60.6 nm.

3.2. Electrochemical characteristics of ZIF-67/GCE, ZIF-67/MWCNT/GCE, MWCNT/GCE

The electrochemical characteristics of bare GCE, ZIF-67, ZIF-67/MWCNT and MWCNT modified electrodes were studied via CV and EIS tests. Fig. 3(a) displays CV curves of the above four electrodes measured at a scan rate of 50 mVs^{-1}. The MWCNT modified electrode exhibits the biggest peak current and the smallest peak potential separation (potential difference between oxidation peak potential and reduction peak potential). Bare GCE with good conductivity also exhibits a relatively big peak current and small peak potential separation. In contrast, after modifying GCE with ZIF-67, the electrode modified with ZIF-67 presents the smallest peak current and largest peak potential separation. The ZIF-67/MWCNT modified electrode's peak current and peak potential separation are intermediate of ZIF-67 and MWCNT modified electrode. The peak current in the CV measurement is relevant to the Aeff (electrochemical effective area). The bigger peak currents of ZIF-67/MWCNT and MWCNT modified electrodes may be ascribed to the large Aeff of MWCNT. It is also well known that the rate constant of electron transfer is inversely proportional to the peak potential separation [36]. Therefore, the MWCNT modified electrode possesses the biggest rate constant of electron transfer. Compared with ZIF-67 modified electrode, ZIF-67/MWCNT modified electrode presents a bigger rate constant of electron transfer, indicating the mixing of MWCNT promotes the electron transfer of ZIF-67. For EIS analysis, the phase angles of the low-frequency components are 45°, indicating that the equivalent circuit model is a well-known Randle circuit. The semi-circular arc at high frequency represents the electron transfer resistance (Rct) of the electron transfer process, and the low-frequency line represents the Warburg impedance (Zw) of the diffusion process. Consequently, bare GCE, MWCNT and ZIF-67/MWCNT modified electrode with a smaller semi-circular arc have a better conductivity than ZIF-67 modified electrode, which is consistent with the CV result. Meanwhile, a series of CV measurements at different scan rates were shown in Fig. 3(c), (d) and (e). And they are in turn an irreversible reaction (slow electron transfer process), a quasi-reversible reaction (intermediate electron transfer process) and a reversible reaction (fast electron transfer process) [37], which respectively correspond to ZIF-67/GCE, ZIF-67/MWCNT/GCE and MWCNT/GCE. This CV result further confirms that MWCNTs play a role by promoting the electron transfer process.

3.3. Selection of electrode modification material

The selection of electrode modification material was based on the SWSV response displayed in Fig. 4(a), the three stripping peaks from negative potential to positive potential are Pb^{2+}, Cu^{2+}, and Hg^{2+} in order. ZIF-67 modified electrode exhibits an over three times peak current value compared to the bare GCE, which is attributed to its good catalytic activity and adsorption property for HMIs. It can be also found that there are no distinct stripping peaks for the electrode modified only with MWCNT without ZIF-67. This may be due to the weaker adsorption of MWCNT than that of ZIF-67 on Pb^{2+} and Cu^{2+}, leading to less Pb and Cu obtained during the electrochemical deposition process. Therefore, there are much weaker stripping peak electrochemical signals when only modified with MWCNT. The response curve, obtained by the MWCNT-modified electrode with a large electrochemical signal but no distinct stripping peaks, confirms that MWCNT plays a role by

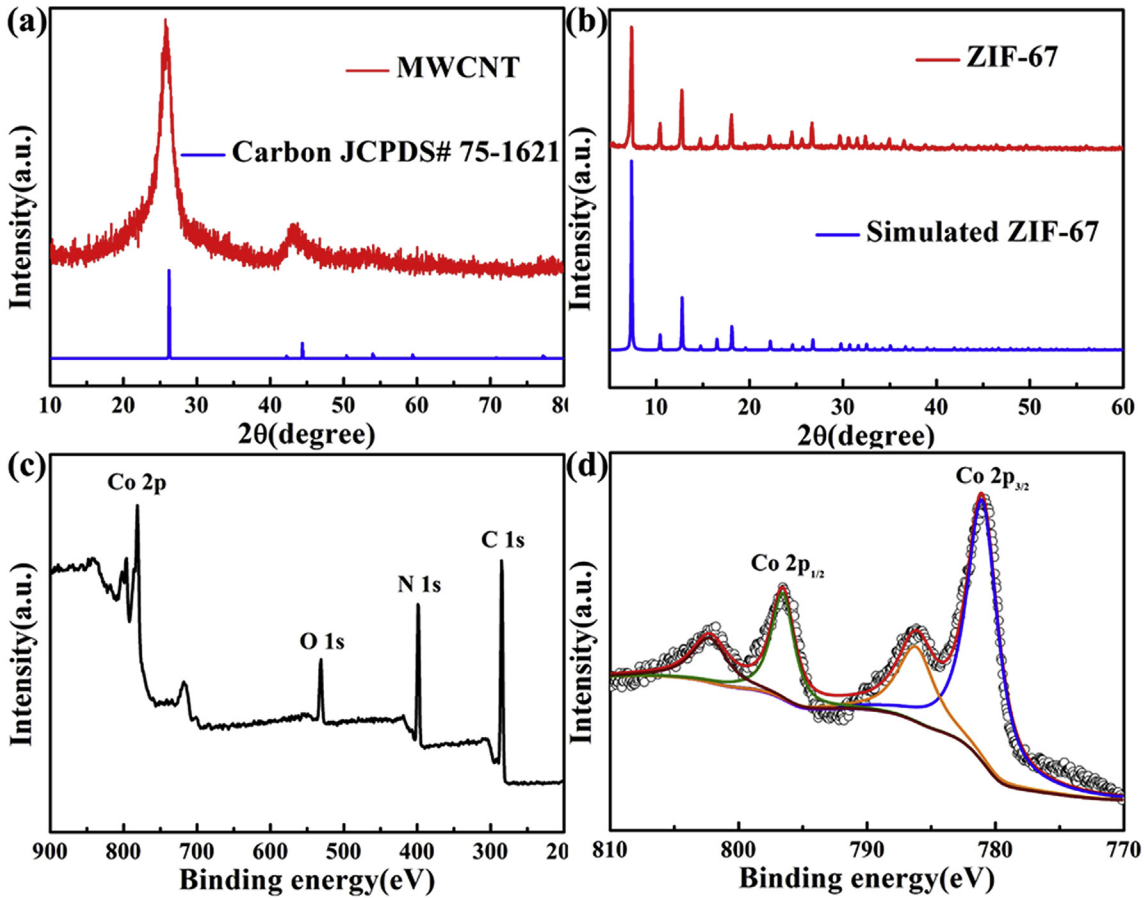

Fig. 1. XRD patterns of (a) MWCNT, (b) ZIF-67; (c) Full XPS spectrum of ZIF-67, (d) high-resolution XPS spectrum of Co 2p.

promoting the electron transfer process and finally increasing the electrochemical signal. It also demonstrates that ZIF-67 is an indispensable part of the electrode modification layer. When MWCNT and ZIF-67 are used together, MWCNT functions to accelerate electron transfer and further increase the response peak current. The stripping peak current of Pb^{2+} and Cu^{2+} increase, while there is no stripping peak of Hg^{2+} after modification of Nafion. Of course, the stripping peak at 0.1 V may also be the common peak of Cu^{2+} and Hg^{2+}. To investigate this, the comparison SWSV test for the electrolytes whether containing Hg^{2+} is shown in Fig. S3. The stripping peak potential and the current value of the two curves at 0.1 V are almost the same, which proves that the inclusion of Hg^{2+} will not change the stripping peak at 0.1 V. Moreover, the addition of Hg^{2+} with a much higher concentration than that of Pb^{2+} and Cu^{2+} also has little effect on the stripping peak currents of both Pb^{2+} and Cu^{2+}, as shown in Table S3. The above results indicate that whether Hg^{2+} is at a high concentration or a low concentration will not affect the stripping peak at 0.1 V, demonstrating that the peak at 0.1 V is not the common peak of Cu^{2+} and Hg^{2+}. According to Hard-Soft-Acid-Base, Pb^{2+} and Cu^{2+} belong to borderline acids, but Hg^{2+} belongs to soft acids. The sulfonic acid group of Nafion belongs to the borderline base, and the binding ability to Pb^{2+} and Cu^{2+} is stronger than that of Hg^{2+}. Therefore, more Pb^{2+} and Cu^{2+} participate in the electrochemical reaction and the stronger signal of Cu^{2+} covers the weak signal of Hg^{2+}. Modification ways of Nafion were simultaneously studied in Fig. 4(b). Both Nafion's mixed and layered modifications enhance the stripping peak current of Pb^{2+} and Cu^{2+}, while Nafion's layered modification shows a stronger effect. Consequently, the sensor, named ZIF-67/MWCNT/Nafion/GCE, was finally fabricated by ZIF-67/MWCNT and Nafion with a layered modification way.

3.4. Optimization

The following parameters were optimized: (a) types of the electrolyte; (b) pH value of the optimized electrolyte; (c) deposition potential; (d) deposition time; The results were shown in Fig. S4. The final optimized conditions were determined as follows: (a) HAc-NaAc; (b) pH value of 2; (c) −0.9 V; (d) 260 s. The detailed discussion is shown in the supporting information.

3.5. Discussion of sensing mechanism

The detection process of Pb^{2+} and Cu^{2+} is as follows: First, set the potential of GCE to the optimal deposition potential of −0.9 V, and electrons are transferred from GCE to Pb^{2+} and Cu^{2+} to obtain Pb and Cu. Then apply a positive voltage to GCE. When the characteristic stripping peak potential (Pb^{2+}: ~-0.6 V and Cu^{2+}: ~-0.1 V) reaching, Pb and Cu begin to transform into Pb^{2+} and Cu^{2+} and return to the solution. At the same time, electrons return to GCE and the detected stripping peak current signal is obtained. In this detection process, the sensing performance mainly depends on Pb^{2+} and Cu^{2+} enrichment and electrons transfer. Based on this we constructed the electrode modification layer system as shown in Fig. 5(a). The modified layer system could be divided into four function parts: GCE, ZIF-67, MWCNT, and Nafion. Nafion, with the electrostatic attraction effect of sulfonic acid groups, has a good enrichment effect on Pb^{2+} and Cu^{2+}. In addition, the good

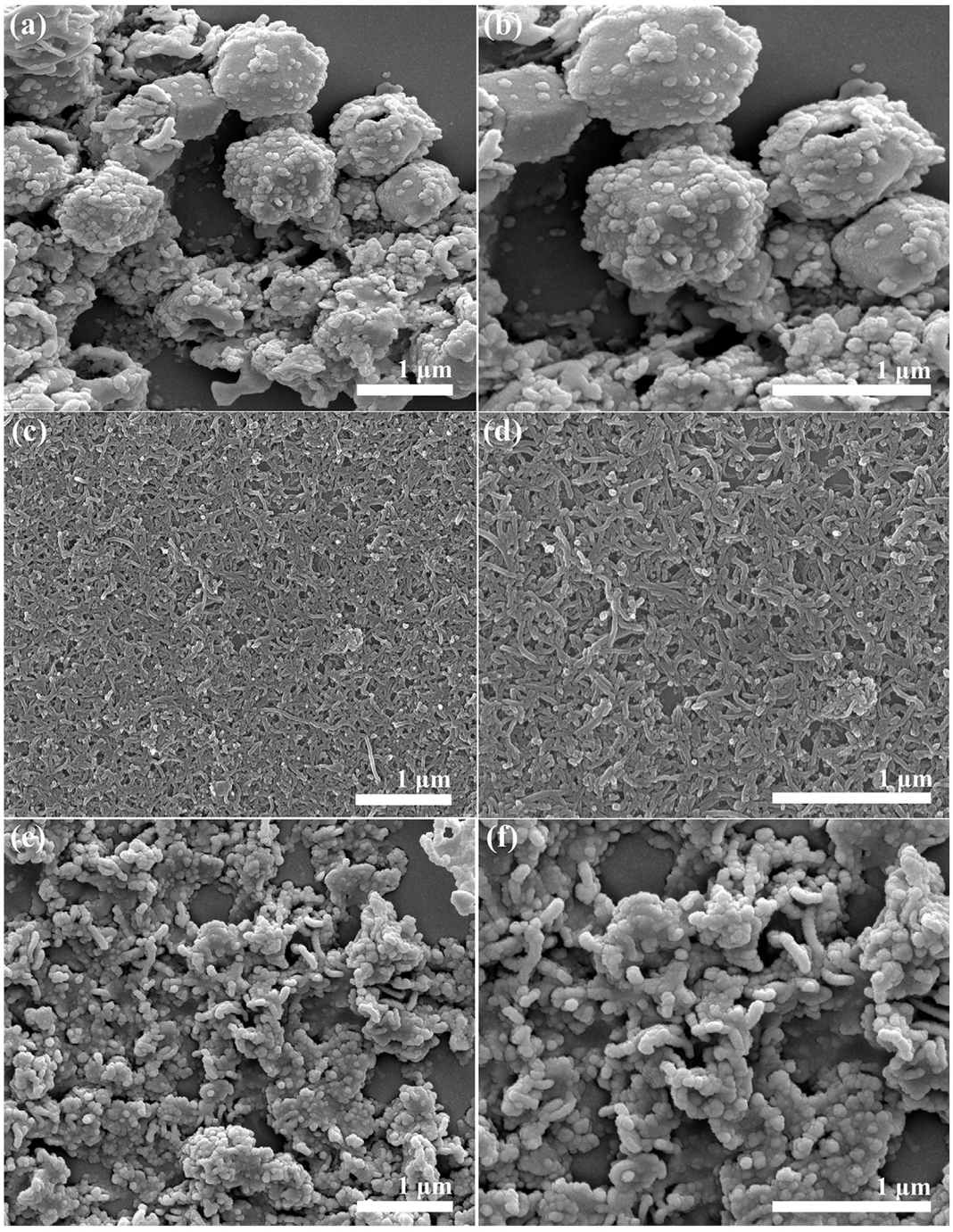

Fig. 2. SEM images of (a), (b) ZIF-67 at different magnifications after ultrasound; (c), (d) MWCNT at different magnifications after ultrasound; (e), (f) ZIF-67/MWCNT at different magnifications after ultrasound.

adsorption of ZIF-67 on HMIs further enriches Pb^{2+} and Cu^{2+} at ZIF-67/MWCNT and Nafion interface. The enrichment of Pb^{2+} and Cu^{2+} at ZIF-67/MWCNT and Nafion interface increases the content of HMIs participating in the electrochemical reaction, which in turn increases the response signal. Electron transfer takes place through the following 2 routes. Take the deposition process as an example. Route a: Electrons are transferred from GCE to Pb^{2+} and Cu^{2+} at the ZIF-67/MWCNT and Nafion interface, and Pb^{2+} and Cu^{2+} are reduced to Pb and Cu. Route b: Co^{2+} in ZIF-67 gets electrons from GCE and turns into Co^{+}. Co^{+} transfers electrons to other Co^{2+} in ZIF-67 to obtain new Co^{+}. Electrons are transferred through the mutual conversion of Co^{2+} and Co^{+}. Finally, Co^{+} near the ZIF-67/MWCNT and Nafion interface transfers electrons to Pb^{2+} and Cu^{2+} to get Pb and Cu. In route a, electrons transfer is accelerated by MWCNT with good conductivity, which has been proven by the CV test shown in Fig. 3. In route b, ZIF-67 and MWCNT synergistically act on the diffusion and transition of electrons. The catalytic action of Co^{2+} provides a new reaction route b, thereby improving the sensing performance of the sensor. To demonstrate this, the effect of Co^{2+} addition was measured using ZIF-67/MWCNT/GCE as shown in Fig. 5(b). '0' represents the HAc-NaAc (pH = 4) only containing Pb^{2+} and Cu^{2+} without Co^{2+}, while '1' and '2' represents the addition of

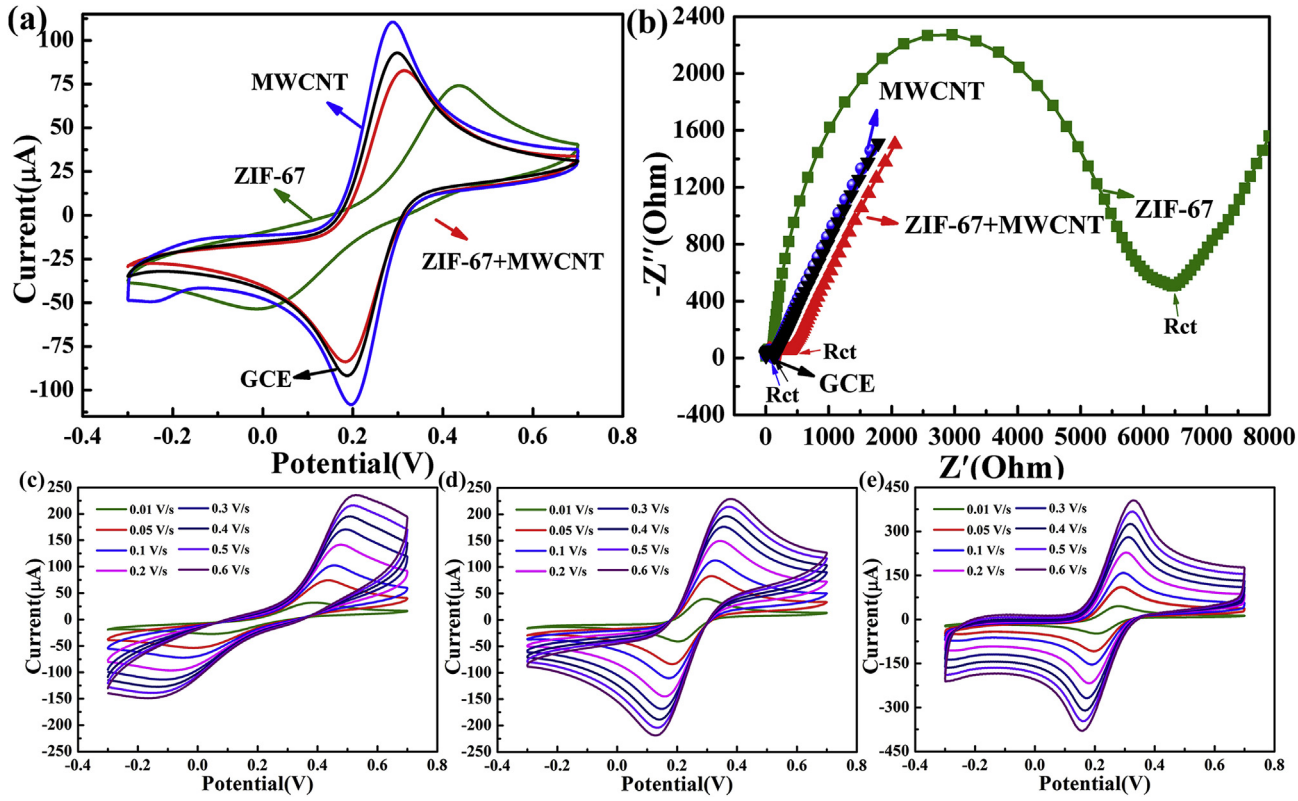

Fig. 3. (a) Cyclic voltammograms and (b) Electrochemical impedance spectra of bare GCE, ZIF-67, ZIF-67/MWCNT and MWCNT modified electrodes in 5 mM $Fe(CN)_6^{3-/4-}$ containing 0.1 M KCl. Cyclic voltammograms at different scan rate of (c) ZIF-67, (d) ZIF-67/MWCNT and (e) MWCNT modified electrodes in 5 mM $Fe(CN)_6^{3-/4-}$ containing 0.1 M KCl.

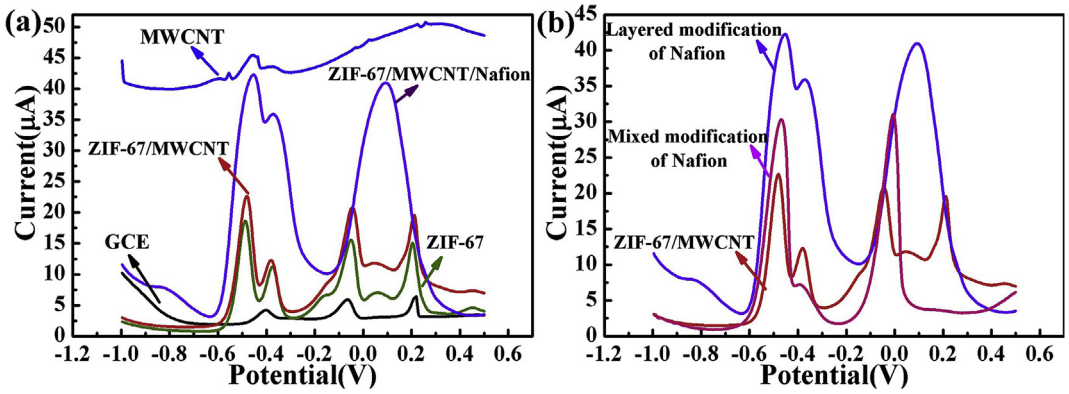

Fig. 4. SWSV curves of (a) different modified material modified electrodes: GCE, ZIF-67/GCE, MWCNT/GCE, ZIF-67/MWCNT/GCE and ZIF-67/MWCNT/Nafion/GCE, (b) different modification ways modified electrodes: ZIF-67/MWCNT/GCE, layered and mixed modification of Nafion modified electrodes.

20 and 40 μM Co^{2+} respectively. The stripping peak current values of Pb^{2+} and Cu^{2+} are positively correlated with the Co^{2+} content, indicating that Co^{2+} has a catalytic effect on the electrochemical reactions of Pb^{2+} and Cu^{2+}. That is, ZIF-67 plays an important catalytic role in the sensing performance of the fabricated sensor. At the same time, it can be found in Fig. 4(b) that when Nafion is modified in different ways, the stripping peak current values of Pb^{2+} and Cu^{2+} are not the same. In order to investigate the reason, chronocoulometry test was performed to compare their adsorption characteristics as shown in Fig. 5(c). When Nafion is modified hierarchically, the rate of charge increment is greater. This indicates the sensor with a layered modification of Nafion has a higher adsorption capacity, further resulting in a bigger stripping peak current of the SWSV test displayed in Fig. 4(b). This result also demonstrates that the maximum exposure extent of Nafion to the Pb^{2+} and Cu^{2+} electrolyte results in a better enrichment effect. Therefore, the construction of the proposed sensor was based on the good electrocatalytic activity of ZIF-67/MWCNT and enrichment effect of Nafion to Pb^{2+} and Cu^{2+}.

3.6. Electrochemical responses of ZIF-67/MWCNT/nafion/GCE

The sensitivity of ZIF-67/MWCNT/Nafion/GCE was investigated under optimal experimental conditions. The SWSV responses of different Pb^{2+} and Cu^{2+} concentrations were shown in Fig. 6(a). Herein, the concentration of Pb^{2+} and Cu^{2+} is from 1.38 nM–5 μM

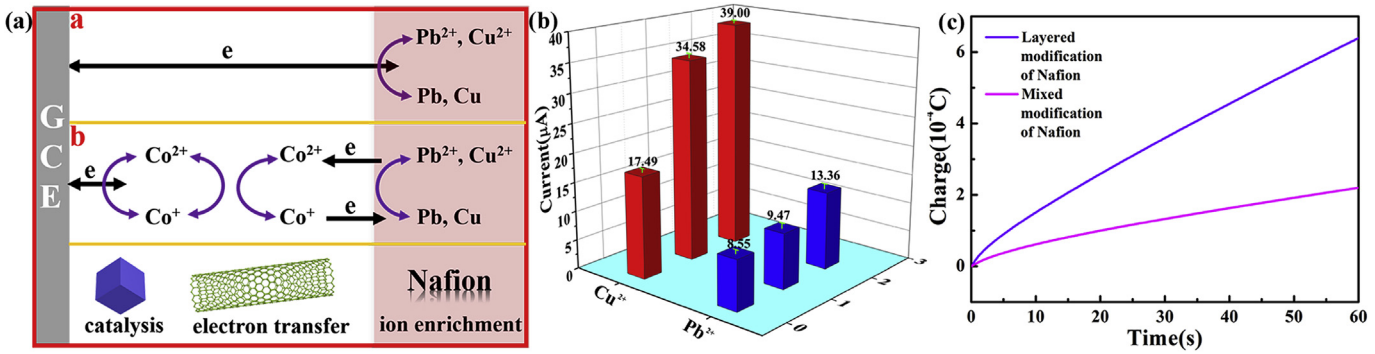

Fig. 5. (a) Function mechanism of ZIF-67/MWCNT/Nafion modified layer; (b) Effects of Co^{2+} addition on the stripping peak current response of Pb^{2+} and Cu^{2+}; (c) Adsorption kinetic curves of layered and mixed modification of Nafion towards Pb^{2+} and Cu^{2+} at 0.6 μM.

and 1.26 nM–5 μM, respectively. Corresponding calibration curves of simultaneously detecting Pb^{2+} and Cu^{2+} were displayed in Fig. 6(b), both showing a good linear relationship in the low concentration range and logarithmic linear relationship in the high concentration range. The linear regression equations toward Pb^{2+} are $y = 63.7234x+5.0773$ ($R^2 = 0.9978$, $x = 0.00138–0.60138$ μM), and $y = 23.7264lgx+50.6128$ ($R^2 = 0.9808$, $x = 0.60138–5.001$ μM). And toward Cu^{2+} are $y = 97.8194x+23.4939$ ($R^2 = 0.9924$, $x = 0.00126–0.20126$ μM), and $y = 10.5379lgx+ 50.4843$ ($R^2 = 0.9975$, $x = 0.20126–5.001$ μM), where x is concentration (μM) of Pb^{2+} and Cu^{2+} and y is stripping peak current (μA)). The theoretical low detection limits (LODs) for Pb^{2+} and Cu^{2+}, based on a signal-to-noise ratio (S/N) = 3, are calculated as ~10 and 3.8 nM. The theoretical result of the LOD is slightly higher than the actual result. Because there is still 1.38 nM Pb^{2+} and 1.26 nM Cu^{2+} in ultrapure water as shown in Table S1(in the supporting information). It is then used as a blank sample in the calculation of LOD. The ultra-sensitive sensor still responds to this trace amount of Pb^{2+} and Cu^{2+}, resulting in a bigger standard deviation of the blank sample and theoretical value of LOD. Consequently, the LODs of Pb^{2+} and Cu^{2+} were finally determined as 1.38 and 1.26 nM of the actual results. The fabricated sensor was also compared with those previously reported, as displayed in Table S2 [38–43]. It can be clearly seen that the fabricated sensor in this work exhibits a promising advantage on sensitivity with comparable or even better characteristics on LODs and linear range. Although the sensitivity of Pb^{2+} is smaller than that of Pd@PAC/GCE, the linear range is much larger than Pd@PAC/GCE. To conclude, combining linearity, sensitivity and detection limits, the fabricated sensor in this work delivers superior performance in the simultaneous detection of Pb^{2+} and Cu^{2+}.

3.7. Repeatability, reproductivity, stability, specificity and interference study

In addition to good sensing performance, repeatability, reproducibility, and anti-interference ability also play an important role in real sample analysis. The repeatability was examined by 10 parallel experiments in 0.1 M pH 2.0 HAc–NaAc solution containing 0.6 μM Pb^{2+} and Cu^{2+}. As shown in Fig. 7(a), the stripping peak currents of 10 parallel experiments remain almost unchanged and the corresponding relative standard deviations (RSD) for Pb^{2+} and Cu^{2+} are calculated to be 3.0% and 2.5%, indicating the fabricated sensor has good stability for repeated detection. As shown in Fig. 7(b), the fabricated sensor also has a good reproducibility with an RSD of 3.6% for Pb^{2+} and 4.4% for Cu^{2+}. In addition, when testing the reproducibility, the modified electrode suspension will be ultrasonicated again before each test, which will result in a different morphology. Therefore, the good reproducibility for Pb^{2+} and Cu^{2+} indicates that morphology has no effect on sensing performance. To evaluate the anti-interference ability, over 50-fold concentrations of other HMIs such as K^+, Na^+, Mg^{2+}, Zn^{2+}, Hg^{2+},

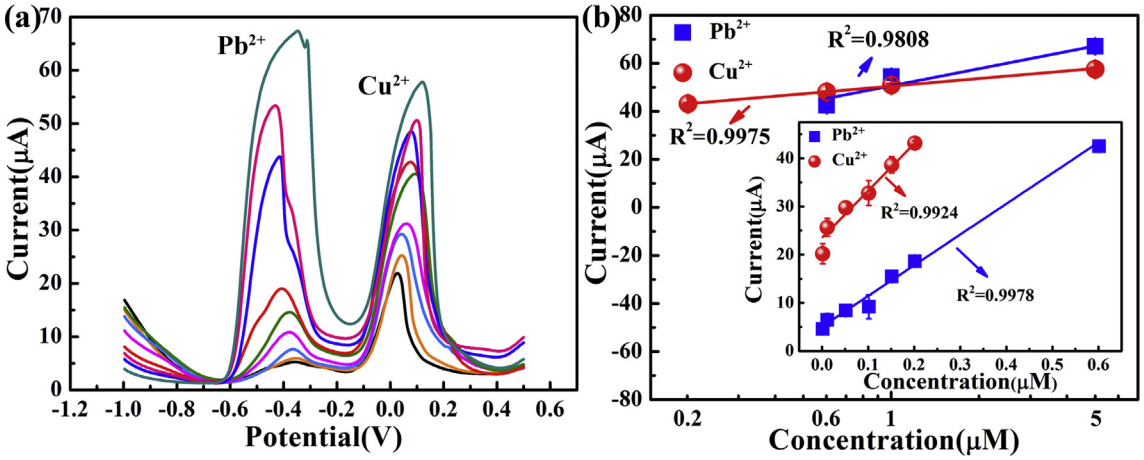

Fig. 6. (a) SWSV curves for different concentrations of Pb^{2+} and Cu^{2+} (b) Linear relationship of stripping peak current with logarithm of Pb^{2+} and Cu^{2+} concentrations in the high concentration range. The inset is the relationship of stripping peak current with Pb^{2+} and Cu^{2+} concentrations in the low concentration range for the sensor attached with ZIF-67/MWCNT/Nafion/GCE.

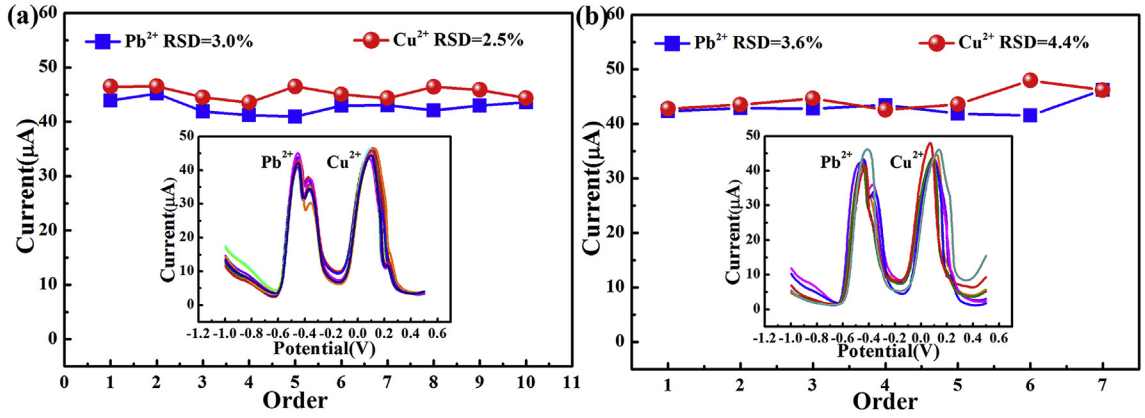

Fig. 7. Evaluation of the (a) repeatability of ZIF-67/MWCNT/Nafion/GCE with 10 consecutive measurements, (b) reproducibility of ZIF-67/MWCNT/Nafion/GCE with seven fabricated sensors.

Fe^{3+}, Co^{2+}, Cd^{2+}, and Mn^{2+} were added. As shown in Table S3 (in the supporting information), the changes of stripping peak currents for both Pb^{2+} and Cu^{2+} are all less than 5%, which implies that the fabricated sensor has a good anti-interference ability. At the same time, it cannot be ignored that when ZIF-67/MWCNT/GCE modified a layer of Nafion, the addition of Co^{2+} did not increase the stripping peak current of Pb^{2+} and Cu^{2+}, which is different from that in Fig. 5(b). This is because this sensor (ZIF-67/MWCNT/Nafion/GCE) has a Nafion modified layer. The Nafion modified layer hinders the diffusion of Co^{2+} to the ZIF-67/MWCNT modified layer, so adding Co^{2+} does not increase the stripping peak current of Pb^{2+} and Cu^{2+}. It also demonstrates that Co^{2+} in the ZIF-67/MWCNT modified layer will not easily dissolve into the solution due to the existence of the Nafion barrier layer, which brings good stability to ZIF-67/MWCNT/Nafion/GCE. The stability of the fabricated sensor was evaluated after 10 days of storage as depicted in Fig. 8(a). There is no distinctive change for the stripping peak current of both Pb^{2+} and Cu^{2+}, demonstrating good stability. Finally, the specificity was tested via obtaining a SWSV curve in the solution containing Ni^{2+}, Pb^{2+}, Fe^{3+}, Cu^{2+}, and Hg^{2+}. The concentration of Ni^{2+}, Fe^{3+}, and Hg^{2+} is 30 μM, which is much higher than the concentration of Pb^{2+} and Cu^{2+}. Since the stripping peak potentials of the three ions Ni^{2+}, Fe^{3+}, and Hg^{2+} are similar to those of Pb^{2+} and Cu^{2+}, they were selected to study the specificity of the fabricated sensor for Pb^{2+} and Cu^{2+}. As shown in Fig. 8(b), the three stripping peaks separately correspond to Pb^{2+}, Cu^{2+}, and Hg^{2+} from negative potential to positive potential, and there are no stripping peaks for other ions. Moreover, the stripping peak current of the fabricated sensor for Pb^{2+} and Cu^{2+} is much higher than that for Hg^{2+}, indicating that the sensor has good specificity for Pb^{2+} and Cu^{2+}.

3.8. Real sample analysis

To further evaluate the feasibility of ZIF-67/MWCNT/Nafion/GCE in the real sample analysis, lake water of Yan Lake (Jilin University) and domestic sewage of Sanjia Lake in Changchun were selected as real samples for quantitative analysis. The real water sample was first filtered by a 0.22 μm membrane, and then mixed with the electrolyte at a ratio of 1:19. Table 1 shows the test results of real water samples, where the added concentration is from the ICP-MS test and the found concentration is the test result of the fabricated sensor. Their ratios, namely recoveries, are determined to be 87%–126% for Pb^{2+} and 94%–106% for Cu^{2+}. When Pb^{2+} is below 2 nM, the recovery for Pb^{2+} is a little bigger value of 126%. When Pb^{2+} is higher than 2 nM, the recovery for both Pb^{2+} and Cu^{2+} is below the range of 80%–120%, indicating a potential application in real sample detection. Meanwhile, the concentration of 2 nM is far below the safety limit of Pb^{2+} (70 nM) [44]. Consequently, the sensor overall exhibits a good recovery characteristic in real sample analysis. These results demonstrate that the present sensor with ZIF-67/MWCNT/Nafion/GCE has a good feasibility for simultaneously detecting Pb^{2+} and Cu^{2+} in real samples.

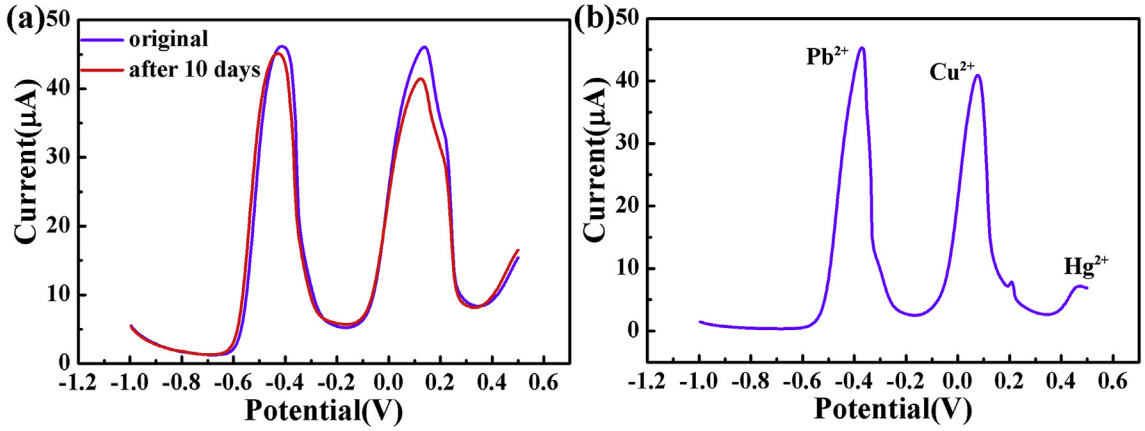

Fig. 8. Evaluation of (a) the stability of ZIF-67/MWCNT/Nafion/GCE after 10 days of storage at room temperature and (b) the specificity of ZIF-67/MWCNT/Nafion/GCE.

Table 1
Recovery measurements of Pb^{2+} and Cu^{2+} in domestic sewage and lake water samples using ZIF-67/MWCNT/Nafion/GCE.

sample	Pb^{2+}			Cu^{2+}		
	added(nM)	found(nM)	recovery(%)	added(nM)	found(nM)	recovery(%)
domestic sewage	1.39	1.74	126	2.50	2.66	106
Yan	1.38	1.74	126	1.66	1.76	106
Lake	51.38	44.54	87	51.26	52.88	103
	101.38	89.50	88	101.26	95.13	94

4. Conclusions

In this study, an electrochemical sensor based on ZIF-67/MWCNT/Nafion/GCE for simultaneous detection of Pb^{2+} and Cu^{2+} was successfully prepared with different facile MLs. The fabricated sensor exhibited an ultrasensitive characteristic in simultaneously detecting Pb^{2+} and Cu^{2+}, which can be ascribed to the good Pb^{2+} and Cu^{2+}adsorption of ZIF-67 and Nafion, the catalytic activity of ZIF-67, and good electronic transfer capability of MWCNT. In addition, it showed a large linear range, ultra-low LOD, good sensitivity, repeatability, reproducibility, anti-interference ability, stability, specificity, and feasibility in real samples. Moreover, all modified materials are easy to synthesize or undergo simple pretreatment, and different MLs' fabrications were by facile physical methods. All in all, these characteristics (such as good and stable sensing performance and facile sensor fabrication) gave the sensor a great potential to simultaneously detect Pb^{2+} and Cu^{2+} in real environments.

Declaration of competing interest

The authors declare that they have no known competing financial interests or personal relationships that could have appeared to influence the work reported in this paper.

CRediT authorship contribution statement

Yueying Zhang: Conceptualization, Data curation, Software, Formal analysis, Writing - original draft. **Hao Yu:** Data curation. **Tong Liu:** Software, Formal analysis. **Weijia Li:** Software, Formal analysis. **Xidong Hao:** Software, Formal analysis. **Qi Lu:** Software, Writing - review & editing. **Xishuang Liang:** Conceptualization, Supervision. **Fengmin Liu:** Validation, Writing - review & editing. **Fangmeng Liu:** Validation, Writing - review & editing. **Chenguang Wang:** Validation, Writing - review & editing. **Chunhua Yang:** Formal analysis. **Hongqiu Zhu:** Formal analysis. **Geyu Lu:** Conceptualization, Supervision.

Acknowledgment

This work was supported by the National Nature Science Foundation of China (Nos. 61533021, 61973134, 61831011 and 61520106003), National Key R&D Program of China (No. 2016YFC0201002), Program for Chang Jiang Scholars and Innovative Research Team in University (No. IRT-17R47), and Application and Basic Research of Jilin Province (20190201276JC), STIRT-JLU(2017TD-07).

Appendix A. Supplementary data

Supplementary data to this article can be found online at https://doi.org/10.1016/j.aca.2020.05.023.

References

[1] L. Ma, Q. Wang, S.M. Islam, Y. Liu, S. Ma, M.G. Kanatzidis, Highly selective and efficient removal of heavy metals by layered double hydroxide intercalated with the $MoS_4^{(2-)}$ ion, J. Am. Chem. Soc. 138 (2016) 2858–2866.
[2] X. Liu, X. Bai, L. Dong, J. Liang, Y. Jin, Y. Wei, Y. Li, S. Huang, J. Qu, Composting enhances the removal of lead ions in aqueous solution by spent mushroom substrate: biosorption and precipitation, J. Clean. Prod. 200 (2018) 1–11.
[3] J. Zhao, Y. Niu, B. Ren, H. Chen, S. Zhang, J. Jin, Y. Zhang, Synthesis of Schiff base functionalized superparamagnetic Fe_3O_4 composites for effective removal of Pb(II) and Cd(II) from aqueous solution, Chem. Eng. J. 347 (2018) 574–584.
[4] L. Jarup, Hazards of heavy metal contamination, Br. Med. Bull. 68 (2003) 167–182.
[5] H.J. Binns, C. Campbell, M.J. Brown, P. Advisory, Comm Childhood Lead, Interpreting and managing blood lead levels of less than 10 μg/dL in children and reducing childhood exposure to lead: recommendations of the Centers for Disease Control and Prevention advisory committee on childhood lead poisoning prevention, Pediatrics 120 (2007) E1285–E1298.
[6] P.G. Georgopoulos, A. Roy, M.J. Yonone-Lioy, R.E. Opiekun, P.J. Lioy, Environmental copper: its dynamics and human exposure issues, J. Toxicol. Environ. Health B Crit. Rev. 4 (2001) 341–394.
[7] C. Arpa, I. Aridasir, Ultrasound assisted ion pair based surfactant-enhanced liquid-liquid microextraction with solidification of floating organic drop combined with flame atomic absorption spectrometry for preconcentration and determination of nickel and cobalt ions in vegetable and herb samples, Food Chem. 284 (2019) 16–22.
[8] A. Yuan, X. Wu, X. Li, C. Hao, C. Xu, H. Kuang, Au@gap@AuAg nanorod side-by-side assemblies for ultrasensitive SERS detection of mercury and its transformation, Small 15 (2019), e1901958.
[9] R.C.d.S. Silva, B.C. Pires, K.B. Borges, Double-imprinted polymer based on cross-linked poly(vinylimidazole–trimethylolpropane trimethacrylate) in solid phase extraction for determination of lead from wastewater samples by UV–vis spectrophotometry, Int. J. Environ. Anal. Chem. 99 (2019) 949–967.
[10] M. Wang, H. Ma, Q. Chi, Q. Li, M. Li, H. Zhang, C. Li, H. Fang, A monolithic copolymer prepared from N-(4-vinyl)-benzyl iminodiacetic acid, divinylbenzene and N,N'-methylene bisacrylamide for preconcentration of cadmium(II) and cobalt(II) from biological samples prior to their determination by ICP-MS, Mikrochim. Acta 186 (2019) 537.
[11] D. Qin, A. Chen, X. Mamat, Y. Li, X. Hu, P. Wang, H. Cheng, Y. Dong, G. Hu, Double-shelled yolk-shell Si@C microspheres based electrochemical sensor for determination of cadmium and lead ions, Anal. Chim. Acta 1078 (2019) 32–41.
[12] C.D. Wu, M. Zhao, Incorporation of molecular catalysts in metal-organic frameworks for highly efficient heterogeneous catalysis, Adv. Mater. 29 (2017) 1605446.
[13] X.-m. Zhang, Z. Zhang, B. Zhang, X. Yang, X. Chang, Z. Zhou, D.-H. Wang, M.-H. Zhang, X.-H. Bu, Synergistic effect of Zr-MOF on phosphomolybdic acid promotes efficient oxidative desulfurization, Appl. Catal. B Environ. 256 (2019) 117804.
[14] Y. Pi, X. Li, Q. Xia, J. Wu, Y. Li, J. Xiao, Z. Li, Adsorptive and photocatalytic removal of Persistent Organic Pollutants (POPs) in water by metal-organic frameworks (MOFs), Chem. Eng. J. 337 (2018) 351–371.
[15] S.Q. Deng, Y.L. Miao, Y.L. Tan, H.N. Fang, Y.T. Li, X.J. Mo, S.L. Cai, J. Fan, W.G. Zhang, S.R. Zheng, An anionic nanotubular metal-organic framework for high-capacity dye adsorption and dye degradation in darkness, Inorg. Chem. 58 (2019) 13979–13987.
[16] S.A.A. Razavi, A. Morsali, Function-structure relationship in metal-organic frameworks for mild, green, and fast catalytic C-C bond formation, Inorg. Chem. 58 (2019) 14429–14439.
[17] M. Feng, P. Zhang, H.C. Zhou, V.K. Sharma, Water-stable metal-organic frameworks for aqueous removal of heavy metals and radionuclides: a review, Chemosphere 209 (2018) 783–800.
[18] N.M. Mahmoodi, M. Taghizadeh, A. Taghizadeh, J. Abdi, B. Hayati, A.A. Shekarchi, Bio-based magnetic metal-organic framework nanocomposite: ultrasound-assisted synthesis and pollutant (heavy metal and dye) removal from aqueous media, Appl. Surf. Sci. 480 (2019) 288–299.
[19] J. Wen, P. He, C. Lei, E. Lv, Y. Wu, J. Gao, J. Yao, Fabrication of metal-organic framework@Yeast composite materials for efficient removal of Pb^{2+} in water, J. Solid State Chem. 274 (2019) 26–31.
[20] Z. Li, G. Zhou, H. Dai, M. Yang, Y. Fu, Y. Ying, Y. Li, Biomineralization-mimetic preparation of hybrid membranes with ultra-high loading of pristine

metal–organic frameworks grown on silk nanofibers for hazard collection in water, J. Mater. Chem. 6 (2018) 3402–3413.
[21] A. Shams, A. Yari, A new sensor consisting of Ag-MWCNT nanocomposite as the sensing element for electrochemical determination of Epirubicin, Sensor. Actuator. B Chem. 286 (2019) 131–138.
[22] B. Sun, J. Liu, A. Cao, W. Song, D. Wang, Interfacial synthesis of ordered and stable covalent organic frameworks on amino-functionalized carbon nanotubes with enhanced electrochemical performance, Chem. Commun. 53 (2017) 6303–6306.
[23] H.V.S. Ganesh, B.R. Patel, H. Fini, A.M. Chow, K. Kerman, Electrochemical detection of gallic acid-capped gold nanoparticles using a multiwalled carbon nanotube-reduced graphene oxide nanocomposite electrode, Anal. Chem. 91 (2019) 10116–10124.
[24] W. Yao, H. Guo, H. Liu, Q. Li, R. Xue, N. Wu, L. Li, M. Wang, W. Yang, Simultaneous electrochemical determination of acetaminophen and dopamine based on metal-organic framework/multiwalled carbon nanotubes-Au@Ag nanocomposites, J. Electrochem. Soc. 166 (2019) B1258–B1267.
[25] Y. Deng, C.J. Seliskar, W.R. Heineman, Electrochemical behavior of $[Re^{I}(DMPE)_3]^{+}$, where DMPE=1,2-Bis(dimethylphosphino)ethane, at perfluorosulfonated ionomer-modified electrodes, Anal. Chem. 69 (1997) 4045–4050.
[26] L. Yu, Q. Zhang, B. Yang, Q. Xu, Q. Xu, X. Hu, Electrochemical sensor construction based on Nafion/calcium lignosulphonate functionalized porous graphene nanocomposite and its application for simultaneous detection of trace Pb^{2+} and Cd^{2+}, Sensor. Actuator. B Chem. 259 (2018) 540–551.
[27] S. Li, B. Yang, C. Wang, J. Wang, Y. Feng, B. Yan, Z. Xiong, Y. Du, A facile and green fabrication of Cu_2O-Au/NG nanocomposites for sensitive electrochemical determination of rutin, J. Electroanal. Chem. 786 (2017) 20–27.
[28] H. Shang, H. Xu, L. Jin, C. Chen, T. Song, C. Wang, Y. Du, Electrochemical-photoelectrochemical dual-mode sensing platform based on advanced Cu_9S_8/polypyrrole/ZIF-67 heterojunction nanohybrid for the robust and selective detection of hydrogen sulfide, Sensor. Actuator. B: Chem. 301 (2019) 127060.
[29] H. Xu, H. Shang, L. Jin, C. Chen, C. Wang, Y. Du, Boosting electrocatalytic oxygen evolution over Prussian blue analog/transition metal dichalcogenide nanoboxes by photo-induced electron transfer, J. Mater. Chem. 7 (2019) 26905–26910.
[30] Y. Lu, X. Pan, N. Li, Z. Hu, S. Chen, Improved performance of quaternized poly(arylene ether ketone)s/graphitic carbon nitride nanosheets composite anion exchange membrane for fuel cell applications, Appl. Surf. Sci. 503 (2020) 144071.
[31] Y. Zhang, Z. Jin, H. Yuan, G. Wang, B. Ma, Well-regulated nickel nanoparticles functional modified ZIF-67 (Co) derived Co_3O_4/CdS p-n heterojunction for efficient photocatalytic hydrogen evolution, Appl. Surf. Sci. 462 (2018) 213–225.
[32] A. Shokuhi Rad, Functionalization of MWCNT by $-SO_3H$ and $-COOH$ groups and their application as solid acidic catalysts for esterification of waste chicken fat, Chem. Biochem. Eng. Q. 31 (2017) 69–75.
[33] Q. Yang, R. Lu, S. Ren, C. Chen, Z. Chen, X. Yang, Three dimensional reduced graphene oxide/ZIF-67 aerogel: effective removal cationic and anionic dyes from water, Chem. Eng. J. 348 (2018) 202–211.
[34] Q. Yang, S. Ren, Q. Zhao, R. Lu, C. Hang, Z. Chen, H. Zheng, Selective separation of methyl orange from water using magnetic ZIF-67 composites, Chem. Eng. J. 333 (2018) 49–57.
[35] L. Xu, Y. Xiong, B. Dang, Z. Ye, C. Jin, Q. Sun, X. Yu, In-situ Anchoring of Fe_3O_4/ZIF-67 Dodecahedrons in Highly Compressible Wood Aerogel with Excellent Microwave Absorption Properties, Materials & Design 182 (2019) 182. UNSP 108006.
[36] X. Gan, H. Zhao, S. Chen, H. Yu, X. Quan, Three-Dimensional porous H_xTiS_2 nanosheet-polyaniline nanocomposite electrodes for directly detecting trace Cu(II) ions, Anal. Chem. 87 (2015) 5605–5613.
[37] J. Wang, Analytical Electrochemistry, third ed., 2006.
[38] X. Zhu, B. Liu, H. Hou, Z. Huang, K.M. Zeinu, L. Huang, X. Yuan, D. Guo, J. Hu, J. Yang, Alkaline intercalation of Ti_3C_2 MXene for simultaneous electrochemical detection of Cd(II), Pb(II), Cu(II) and Hg(II), Electrochim. Acta 248 (2017) 46–57.
[39] X. Han, Z. Meng, H. Zhang, J. Zheng, Fullerene-based anodic stripping voltammetry for simultaneous determination of Hg(II), Cu(II), Pb(II) and Cd(II) in foodstuff, Mikrochim. Acta 185 (2018) 274.
[40] M. Lu, Y. Deng, Y. Luo, J. Lv, T. Li, J. Xu, S.W. Chen, J. Wang, Graphene aerogel-metal-organic framework-based electrochemical method for simultaneous detection of multiple heavy-metal ions, Anal. Chem. 91 (2019) 888–895.
[41] W. Wu, M. Jia, Z. Wang, W. Zhang, Q. Zhang, G. Liu, Z. Zhang, P. Li, Simultaneous voltammetric determination of cadmium(II), lead(II), mercury(II), zinc(II), and copper(II) using a glassy carbon electrode modified with magnetite (Fe_3O_4) nanoparticles and fluorinated multiwalled carbon nanotubes, Mikrochim. Acta 186 (2019) 97.
[42] T. Zhang, H. Jin, Y. Fang, J. Guan, S. Ma, Y. Pan, M. Zhang, H. Zhu, X. Liu, M. Du, Detection of trace Cd^{2+}, Pb^{2+} and Cu^{2+} ions via porous activated carbon supported palladium nanoparticles modified electrodes using SWASV, Mater. Chem. Phys. 225 (2019) 433–442.
[43] S.A. Kitte, S. Li, A. Nsabimana, W. Gao, J. Lai, Z. Liu, G. Xu, Stainless steel electrode for simultaneous stripping analysis of Cd(II), Pb(II), Cu(II) and Hg(II), Talanta 191 (2019) 485–490.
[44] Z. Khoshbin, M.R. Housaindokht, M. Izadyar, A. Verdian, M.R. Bozorgmehr, A simple paper-based aptasensor for ultrasensitive detection of lead (II) ion, Anal. Chim. Acta 1071 (2019) 70–77.